

Spin-polaron band structure and hole pockets in underdoped cuprates

P. Wrobel¹, W. Sulej¹ and R. Eder²¹Institute for the Low Temperature and Structure Research,
P.O. Box 1410, 50-950 Wrocław 2, Poland
and²Forschungszentrum Karlsruhe,
Institut für Festkörperphysik, P.O. Box 3640,
D-76021 Karlsruhe, Germany

We present a variational approach based on the string picture to analyze the internal structure and dispersion of spin polarons with different symmetries in an antiferromagnet. We then use this to discuss the properties of underdoped cuprate superconductor within the 'doped insulator' picture. The theory explains the remnant Fermi surface for the undoped compounds, as well as hole pockets, Fermi arcs, high energy pseudogap and the mid-infrared band in doped materials. Destructive interference between the phases of a photohole near Γ and the internal phases of the Zhang-Rice singlet combined with our theory moreover explains the 'waterfall' phenomenon.

PACS numbers: 71.27.+a, 71.10.Fd, 74.72.-h

I. INTRODUCTION

Since the discovery of high temperature superconductivity (HTSC) in doped antiferromagnetic (AF) insulators, the research on that phenomenon concentrates to a great extent on the properties of single-particle-like excitations in such systems. It is also obvious that the microscopic mechanism of HTSC should hinge on the interaction between quasiparticles. At half filling the Hubbard model, which is a generic model used to describe strongly correlated systems, is an insulator for large enough $U=t[1]$ whereas for low electron density the model is expected to be a Fermi liquid with a Fermi surface volume in accordance with the Luttinger theorem for any $U=t[2]$. With increasing doping one might therefore expect a phase transition from a 'correlation dominated' phase near half-filling to a Fermi-liquid phase for low density. The key property of the correlation dominated phase thereby is the splitting of the physical electron into the two Hubbard bands which correspond to Fermi ion holes and double occupancies moving in a 'background' of singly occupied sites, whereby the electrons forming the background retain only their spin degrees of freedom. This – and not a half-filled Fermi surface – is the picture underlying all successful theories for the angle resolved photoemission spectroscopy (ARPES) data [3] obtained in insulating compounds [4, 5, 6, 7, 8, 9, 10, 11, 12]. The question then is to what extent these Hubbard bands can be doped before the two-band structure collapses, the spin background 'melts' into a Fermi sea and the Luttinger Fermi surface is regained. The key property of this 'doped insulator' phase should be a Fermi surface with a volume proportional to the number of doped holes because these are the only mobile Fermi ions.

ARPES on cuprate superconductors has produced a wealth of information [13] although it has proven difficult to extract a consistent picture. From spectra taken near optimal doping it was concluded that ARPES shows evidence for a 'large' Fermi surface consistent with the Luttinger

theorem and band calculations [13] which would imply that the doped Hubbard bands never exist. Surprisingly enough, however, insulating compounds such as $\text{Sr}_2\text{CuO}_2\text{Cl}_2$ seemed to show a very similar Fermi surface as well – which has been termed the 'remnant Fermi surface' [14]. ARPES spectra from insulators show a band which disperses towards lower binding energy and then rapidly loses weight just as if it would cross a Fermi level. The only possible explanation for this phenomenon is a strong and systematic variation of the spectral weight of the conduction band which drops to near zero abruptly at a line in k -space which roughly coincides with the non-interacting Fermi surface. One can give simple arguments why such a behaviour is to be expected [15]. Since there is no reason why such a strong variation of spectral weight and bands with almost no spectral weight should occur only in insulators one should be cautioned that Fermi surface maps for doped compounds may not show the full picture either.

In the underdoped compounds the upper Hubbard band, while rapidly losing spectral weight, still can be clearly resolved [16]. ARPES shows rather structureless spectra which are usually interpreted in terms of a 'high energy feature' and a 'leading edge shift' or, alternatively, a high energy and low energy pseudogap [13]. In any case there is definitely no 'large' Fermi surface, instead Fermi surface maps show 'Fermi arcs'. Bearing in mind the remnant Fermi surface in the insulators suggests to interpret these arcs as being the inner part of a hole pocket centered on $(\frac{\pi}{2}; \frac{\pi}{2})$ with the part of the pocket facing $(\frac{\pi}{2}; \frac{\pi}{2})$ having too small spectral weight to be seen in ARPES. Assuming that the electronic structure in the underdoped compound can be described in simplest approximation as holes doped into the quasiparticle band of the insulator moreover would give an explanation for the high energy pseudogap – the dispersion of the 'high energy feature' – in that it simply reflects the hole dispersion in the insulator [13]. Such a 'strict' rigid band picture would not explain the low energy pseudogap or the tempera-

ture and doping dependence of either high or low energy pseudogap. On the other hand the closing of the pseudogap with increasing doping can be seen already in cluster simulations[17] and it has been pointed out there that the mechanism may be an effective downward renormalization of the t^0 and t^{00} terms due to decrease in the spin correlation length. Moreover, the low energy pseudogap by its definition in terms of the leading edge shift has no immediate connection with a dispersion and may be determined e.g. by T-dependent linewidths as discussed by Storey et al.[18].

The compound $\text{Ca}_{2-x}\text{Na}_x\text{CuO}_{2-x}\text{Cl}_x$ shows rather clear evidence for the doped insulator picture[19] in that the dispersion in the doped case is virtually identical to that in the undoped compound and even the part of the quasiparticle band facing (π, π) may have been observed. Very recently ARPES experiments seem to have provided direct evidence for hole pockets in $\text{La}_{1.48}\text{Nd}_{0.4}\text{Sr}_{0.12}\text{CuO}_4$ [20], with the part of the pockets facing (π, π) indeed having small spectral weight – as one would have expected on the basis of the remnant Fermi surface.

It had been noted early on [21] that hole pockets with a volume proportional to the hole concentration would explain the scaling of the low temperature Hall constant with hole concentration in the underdoped materials [22, 23] and that the apparent discrepancy between the ‘small Fermi surface’ suggested by transport measurements and the ‘large Fermi surface’ seen in ARPES may be due to a systematic variation of the quasiparticle weight along the hole pocket.[24]. While the recent discovery [25, 26, 27] of Shubnikov-deHaas oscillations in some underdoped compounds initially seemed to provide strong evidence for hole pockets the finding that the oscillations are likely caused by electron-like rather than hole-like pockets[28] has complicated matters again.

Lastly, exact diagonalization studies of the t-J model provide clear evidence that the Fermi surface for hole dopings around 10% takes the form of hole pockets[29, 30]. Careful analysis of exact diagonalization results shows that the single particle spectral function for the doped t-J model is quite consistent with rigid band filling of the quasiparticle band seen at half-filling, provided one takes into account the formation of hole pairs[24]. By calculating the spectral function for dressed hole operators[31] rather than the bare electron operators it can moreover be shown that the quasiparticles in the doped system have very nearly the same internal structure as in the undoped one[32].

Here we take the point of view that the underdoped regime in high-temperature superconductors precisely corresponds to the doped insulator phase. We show that many properties of the underdoped phase – the remnant Fermi surface, the Fermi arcs, the high-energy feature seen in ARPES, the mid infrared band seen in the optical conductivity – find a simple and natural explanation in the dispersion and internal structure of the quasiparticles which correspond to holes heavily dressed by spin

excitations. Since there are indications that the heavily overdoped phase is essentially a Fermi liquid this would imply that the phase transition from the correlated doped phase to the Fermi liquid phase occurs at optimal doping. This would then be a quantum phase transition where none of the two phases has any kind of order – rather they differ in the topology and volume of their Fermi surfaces. An indication of this transition can in fact be seen in the dynamical spin and density correlation function obtained by exact diagonalization of small clusters. In the underdoped regime spin and density correlation functions are very different and the density correlation function takes the form of extended incoherent continua[33]. This form of the density correlation function can be explained quantitatively within the string picture for a single hole[34]. For doping levels higher than optimal, spin and density correlation function become similar and can be explained well as particle-hole transitions across an essentially free-electron-like Fermi surface[35].

While a theory for such a transition would be highly desirable but very challenging the present paper has a more modest goal: we want to show that many features of undoped and underdoped cuprates can be explained by a very simple theory which assumes continuity with the insulator. The calculation will be performed in the framework of the t-J model[36, 37] extended by terms enabling hopping to second and third nearest neighbors with hopping integrals t^0 and t^{00} respectively [38, 39]. We use standard values $t = 0.35\text{eV}$, $t^0 = 0.12\text{eV}$, $t^{00} = 0.08\text{eV}$, and $J = 0.14\text{eV}$ chosen so as to reproduce the measured Fermi surface of hole doped cuprates for high doping levels.

II. CONSTRUCTION OF LOCALIZED BASIS STATES

Since we want to study the doped insulator we consider the motion of a single hole in an antiferromagnetically ordered ‘spin background’. All processes analyzed in the following actually require only short range antiferromagnetic correlations – one may therefore expect that hole motion in a state with short range antiferromagnetic order but no long range order will involve very similar processes so that e.g. the internal structure of the quasiparticles and the dispersion relation of a hole should not change drastically. The construction of spin polaron (SP) states including the excited states was performed in several earlier publications [40, 41, 42, 43, 44]. In order to make this paper self-contained we will now briefly repeat that construction. For definiteness we will assume that a \uparrow -spin has been removed from the system and study the motion of the resulting hole. We denote the \uparrow -sublattice by A.

To begin with we define $H_0 = H_t + H_{\text{Ising}}$ to be the sum of the nearest neighbor hopping t and the longi-

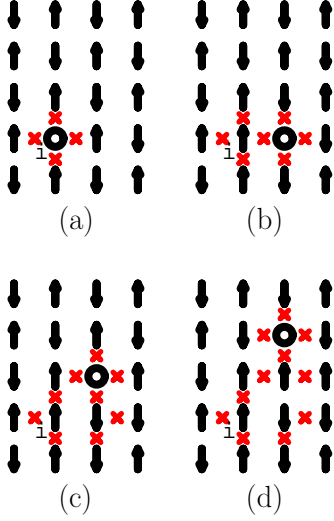


FIG. 1: (Color online) The mechanism of the string effect. Slanted crosses represent links with the contribution to the Ising part of the exchange energy higher by $J=2$ as compared to the Neel state. (b), a string state obtained by a single move of the hole created at site i . (c), (d), states obtained respectively by two and three consecutive moves.

tudinal part of the Heisenberg exchange:

$$H_t = t \sum_{\langle i,j \rangle} (\hat{c}_i^\dagger \hat{c}_j + \text{H.c.});$$

$$H_{\text{Ising}} = J \sum_{\langle i,j \rangle} (S_i^z S_j^z - \frac{n_i n_j}{4});$$

H_0 is frequently referred to as the $t - J_z$ model. In a first step, we seek approximate eigenstates of H_0 which are localized due to the string effect.

The mechanism of the string effect is shown in Fig.1. By creating a hole in the Neel state - i.e. the ground state of H_{Ising} - at site i and acting repeatedly with the hopping term we generate a basis of string states $|\mathcal{P}_i\rangle$ where $\mathcal{P}_i = (i; j; ::; n)$ is shorthand for the sites $i; j; ::; n$ visited by the hole. All spins on these sites have been displaced by one lattice spacing and thus are inverted relative to the Neel order.

All $|\mathcal{P}_i\rangle$ are eigenstates of H_{Ising} . Taking the energy of the string with length 0 i.e. the bare hole as the zero of energy and denoting by l the length of the string - i.e. the number of shifted spins - the eigenvalue is

$$E = \frac{J}{2} (2l + 1) \quad (1)$$

This is exact for $l=2$ and is true for most longer strings as well. For simplicity we assume (1) to be true for any string. This implies that the hole is trapped in a linearly ascending potential and all eigenstates of H_0 are localized. The main deviations from (1) occur for 'loops' as discussed by Trugman [4] which in fact lead to hole-propagation even in the $t - J_z$ model. Such loops pose no

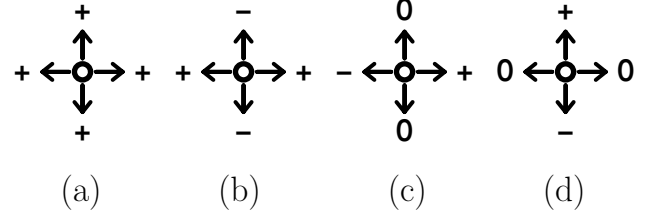


FIG. 2: Dependence of the sign of a given path on the direction of the first move for the $d_{x^2-y^2}$ -wave SP, (b), p_x -wave SP, (c), and p_y -wave SP, (d). For completeness the schematic representation for the s-wave SP has also been shown, (a).

fundamental problem for the present formalism and can be dealt with by introducing the concept of 'irreducible paths' as discussed in detail in Ref. [40].

Next we note that by acting with a point group operation, which leaves the initial site i invariant, the string states $|\mathcal{P}_i\rangle$ are transformed into one another. We can therefore define linear combinations of the $|\mathcal{P}_i\rangle$ which transform like the basis states of the irreducible representations of C_{4v} under these point group operations. Then we make the following ansatz for a localized eigenstate of H_0

$$|j_i^{(o,m)}\rangle = \sum_{\mathcal{P}_i} \langle \mathcal{P}_i^{(o,m)} | j_i^{(o,m)} \rangle |\mathcal{P}_i\rangle; \quad (2)$$

where $o \in \{s, p_x, p_y, d_{x^2-y^2}, d_{xy}\}$ denotes the symmetry or 'orbital character' of the state and m labels the excitation number for a given symmetry. In keeping with (1) we moreover assume that each coefficient $\langle \mathcal{P}_i^{(o,m)} | j_i^{(o,m)} \rangle$ can be factorized into a sign $\langle \mathcal{P}_i^{(o)} | j_i^{(o,m)} \rangle$ - which plays the role of an 'angular wave function' - and a 'radial wave function' $\langle \mathcal{P}_i^{(o,m)} | j_i^{(o,m)} \rangle$ which depends only on the length of the string:

$$\langle \mathcal{P}_i^{(o,m)} | j_i^{(o,m)} \rangle = \langle \mathcal{P}_i^{(o)} | j_i^{(o,m)} \rangle \quad (3)$$

For an A_1 (s-wave) state the sign $\langle \mathcal{P}_i^{(o)} | j_i^{(o,m)} \rangle$ is obviously uniform for all paths. For an E (p-wave) or B_1 ($d_{x^2-y^2}$ -wave) state $\langle \mathcal{P}_i^{(o)} | j_i^{(o,m)} \rangle$ is determined by the direction of the first hop away from the site i as shown in Figure 2. The string of length 0 i.e. the bare hole at site i is invariant under all point group operations and hence has nonvanishing weight only in the s-like state - this implies that E and B_1 states are higher in energy than the A_1 state because they are composed of strings with length ≥ 1 and hence a minimum of three frustrated bonds. For the two remaining representations A_2 (g-wave) and B_2 (d_{xy} -wave) it can be shown that only strings with a minimum length of 2 have nonvanishing weight in the corresponding SP states - these states therefore are even higher in energy and we omit them. For each symmetry sector o we can now set up the Schrodinger equation

$$H_0 |j_i^{(o,m)}\rangle = E |j_i^{(o,m)}\rangle \quad (4)$$

thereby assuming (1) and solve for the eigenenergies $E^{(0;m)}$ and the coefficients – this is explained in Appendix A. As expected for a linearly ascending potential, the ϕ 's are rapidly decreasing with increasing length of the string even for the physical parameter range $t=J=3$. It turns out the Schrodinger equation for the coefficients for the $d_{x^2-y^2}$ SP is identical to that for the p-like ones. To shorten the notation we call the coefficients $c_{(s;0)}$ for the lowest s-like SP and instead of those for the p-like SP, $c_{(p;0)}$ and $d_{x^2-y^2}$ -like SP, $c_{(d;0)}$ we use $c_{(p;0)} = \frac{p}{2}$ and $c_{(d;0)} = 2$ respectively.

III. EFFECTIVE MULTIBAND MODEL FOR SPIN POLARONS

So far we have found SP states (2) which form a set of approximate localized eigenstates of H_0 at each of the sites of the sublattice A. Next we note that the remaining part H_1 of the tJM – which comprises the transverse part of the Heisenberg exchange and the hopping terms $/t^0; t^0$ – has nonvanishing matrix elements between SP states centered on neighboring sites i and j . One important mechanism leading to such a matrix element is the truncation of the string shown in Figure 3. By flipping the first two spins of the defect string the starting point of the string is shifted to a second or third nearest neighbor while the length of the string is reduced by two. Since the coefficients $c_{(p;0)}^{(0;m)}$ and $c_{(p;0)}^{(0;0)}$ of the initial and final string are known by solution of (4) and the strength of the spin-flip term is $J=2$ the corresponding matrix element is easily evaluated. Similarly, the hopping terms $/t^0; t^0$ allow for the hopping of the bare hole between the sites of one sublattice (see Figure 3). In addition there is the 'loop hopping' [4] and actually a wide variety of additional processes, which are discussed in Appendix A.

Assuming that the matrix elements are known we define Fourier transforms

$$j^{(i)}(k) = \frac{1}{N} \sum_{j \in A} j_j^{(i)} e^{ik \cdot R_j} \quad (5)$$

where $i = (0;m)$. Next we make the LCAO-like ansatz for a propagating single-hole state

$$j_1(k) = \sum_i v^{(1)}(k) j_j^{(i)}(k) \quad (6)$$

which leads to a generalized eigenvalue problem of the form

$$H_{\text{eff}}(k) v_1(k) = E_1(k) O_{\text{eff}}(k) v_1(k) \quad (7)$$

where the Hamilton and overlap matrices are given by

$$H_{(i;0)} = \epsilon_0 E^{(i;0)} + T^{(i;0)}(k); \quad (8)$$

$$O_{(i;0)} = 1 + O^{(i;0)}(k) \quad (9)$$

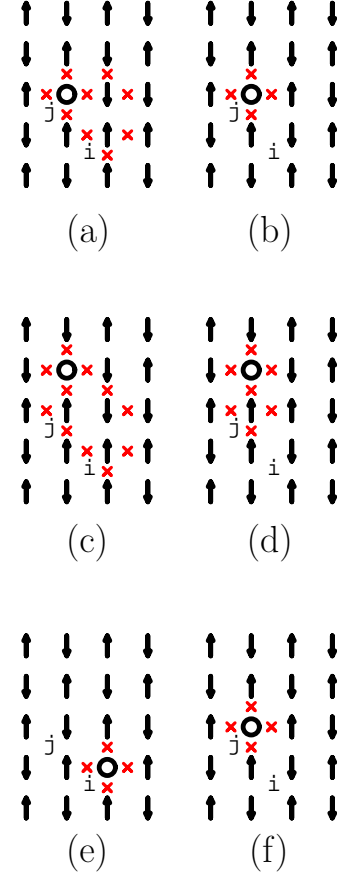


FIG. 3: (Color online) (a) ! (b): a string of length 2 starting at i is truncated to a string of length 0 at j by the transverse part of the Heisenberg exchange. (c) ! (d) a string of length 3 is reduced to one of length 1. (e) ! (f) a bare hole at site i (string of length 0) is transported to j by t^0 -hopping.

and we have introduced the Fourier transform of

$$T_{ii^0}^{(i;0)} = h_{i^0}^{(i;0)} H_{1j}^{(i;0)} i; \quad (10)$$

$$O_{ii^0}^{(i;0)} = h_{i^0}^{(i;0)} j_{i^0}^{(i;0)} i; \quad (11)$$

All these matrix elements can be expressed in terms of the coefficients $c_{(i;0)}$ as discussed in the Appendix A. Once these matrix elements are calculated we readily obtain the band structure for the spin polarons.

To conclude this section we briefly discuss the relationship with previous work. Several authors have studied hole motion in an antiferromagnet by calculations within a string basis [4, 45, 46, 47]. The difference is that the diagonalization of H_0 leads to a considerable reduction of basis states in that high lying eigenstate of H_0 are eliminated from the very beginning. The matrices to be diagonalized in the present work are 4×4 or 10×10 – which is very small compared to the matrix dimensions

in Refs. [4, 45, 46, 47, 48]. Moreover the LCAO-like scheme makes it easier to extract a physical picture. Another frequently applied approach is the self-consistent Born approximation [7, 8, 9, 10, 11, 12, 49, 50, 51]. The single-hole wave function associated with this approximation actually also can be interpreted as a superposition of string states once the Fourier-transformed version of the wave function in Ref. [52] is converted into real space. This explains why the results e.g. for the dispersion of a single hole are practically identical.

IV. PHOTOEMISSION SPECTRA AND FERMI SURFACE

ARPES gives the information on the one-electron removal part of the spectral function defined, at $T = 0$, as

$$A(\mathbf{k};!) = \frac{1}{\pi} \text{Im} \langle \langle \hat{c}_{\mathbf{k};\#}^\dagger \frac{1}{H + i0^+} \hat{c}_{\mathbf{k};\#} \rangle \rangle_{\text{AF}} \quad (12)$$

$|\text{j}_{\text{AF}}\rangle$ represents in (12) the half-filled ground state in which the photoemission process takes place. Since we assume that the rigid band scenario is applicable to cuprates in the low doping range we expect that the conclusions drawn from that analysis are also to some extent applicable to doped systems.

As a first step we approximate the resolvent operator $(\langle H + i0^+ \rangle)^{-1}$ by

$$\frac{1}{\langle H + i0^+ \rangle} \approx \sum_{\mathbf{l};\mathbf{k}} \frac{\langle \text{j}_{\mathbf{l}}(\mathbf{k}) | \hat{H} | \text{j}_{\mathbf{l}}(\mathbf{k}) \rangle}{E_{\mathbf{l}}(\mathbf{k}) + i0^+} \quad (13)$$

i.e. we restrict the single hole states to the coherent superposition of SP states (6).

Next, we have to choose an approximate ground state $|\text{j}_{\text{AF}}\rangle$ of the Heisenberg antiferromagnet. The simplest choice would be the Neel state $|\text{j}_{\text{N}}\rangle$ but in this way we would miss an important mechanism for a \mathbf{k} -dependent quasiparticle weight, namely the coupling of the photo-hole to quantum spin fluctuations. By generating a hole in the Neel state we can obtain only a bare hole, i.e. the string of length 0. In the presence of quantum spin fluctuations the photoemission process can also generate strings of length 1 or 2 – see Figure 4. Since in such a process the hole is created not at the central site i of the SP state – which determines the phase factor $e^{i\mathbf{k} \cdot \mathbf{R}_i}$ in the Bloch state (5) – the photoemission matrix element becomes \mathbf{k} -dependent. Generally speaking the fact that the SP quasiparticles extend over more than one unit cell in real space results in a ‘structure factor’ which varies within the first Brillouin zone in \mathbf{k} -space. As will be seen below, this very \mathbf{k} -dependence is the source of the remnant Fermi surface. In order to capture this effect we use simple first order perturbation theory for the quantum spin fluctuations and set

$$|\text{j}_{\text{AF}}\rangle = |\text{j}_{\text{N}}\rangle - \frac{1}{3} \sum_{\mathbf{h};\mathbf{j}} (S_i^+ S_j + \text{H.c.}) |\text{j}_{\text{N}}\rangle \quad (14)$$

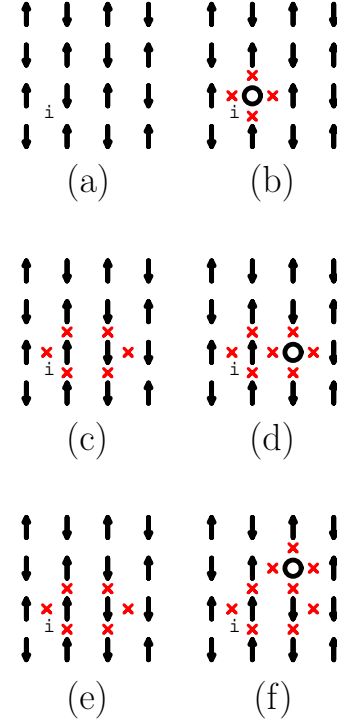


FIG. 4: (Color online) (a) ! (b): Creation of a bare hole at site i from the Neel state. (c) ! (d): Creation of a string of length 1 starting at i from the Neel state + quantum fluctuation. (e) ! (f): Creation of a string of length 2 starting at i from the Neel state + quantum fluctuation.

Since second order perturbation theory gives quite a good estimate for the ground state energy of the Heisenberg antiferromagnet we expect that the probability for coupling to a quantum fluctuation with the electron annihilation operator is described quite well by (14).

Since a quantum fluctuation in the initial states simply gives rise to an extra factor of $1/3$ we immediately obtain the following expressions for the photoemission

matrix element $m^{(i)} = \langle j_{AF} | \hat{p}_k | j_{AF} \rangle$

$$\begin{aligned}
 m^{(s)}(k) &= \frac{2}{3} (\cos(k_x) + \cos(k_y)) \\
 m^{(p_x)}(k) &= \frac{4}{3} ((\cos(k_x) + \cos(k_y)) \cos(k_z)) \\
 &\quad + \frac{2}{3} \sin(k_x) \sin(k_y) \sin(k_z) \\
 m^{(d)}(k) &= \frac{1}{3} (\cos(k_x) - \cos(k_y)) \\
 &\quad + \frac{2}{3} (\cos(2k_x) - \cos(2k_y)) \quad (15)
 \end{aligned}$$

Using these matrix elements we can now compute the spectral density from the normalized SP eigenfunctions.

If we want to compare to experiment, however, there is yet another important effect we need to take into account, namely the coupling of the photohole to charge fluctuations. We may expect that the ground state of the system has not only quantum spin fluctuations but also charge fluctuations i.e. an admixture of pairs of holes and double occupancies with a density $\propto (t/U)^2$. By annihilating an electron on a doubly occupied site it is possible to create a string state with an initial site i by annihilating an electron at a site different from i . Again, this will give rise to a k -dependence of the spectral weight. Such processes actually are not described by the tJM, but since it is rather easy to discuss them we do so. We treat the charge fluctuations in perturbation theory i.e. we replace

$$j_{AF} | \hat{c}_i^\dagger | j_{AF} \rangle + \frac{t}{U} \sum_{hji} \hat{c}_i^\dagger \hat{c}_j | j_{AF} \rangle \quad (16)$$

where $\hat{c}_i^\dagger = \hat{c}_i^\dagger n_i$. The hopping terms t/U do not produce charge fluctuations in the Neel state. Denoting $t/U = J/(4t)$ we get the following correction to the matrix element $m^{(s)}$

$$m^{(s)}(k) = \frac{2}{3} (\cos(k_x) + \cos(k_y)) \quad (17)$$

whereas the corrections to $m^{(p_x)}$ and $m^{(d)}$ are zero. It might appear that the corrections due to charge fluctuations are quite small, being anyway $\propto t/U$. On the other hand, by coupling to charge fluctuations a bare hole at site i can be created by actually annihilating an electron on any of its z neighbors. By changing from $k = (0,0)$ to $k = (\pi, \pi)$ the corresponding contribution to the photoemission matrix element thus changes from $2t/U$ to $4t/U$ and since this has to be added before squaring the matrix element the impact of the charge fluctuations is in fact quite strong. The way in which we are treating charge fluctuations would be adequate for a simple one-band Hubbard model, which is not the proper model for cuprate superconductors. A very similar calculation for

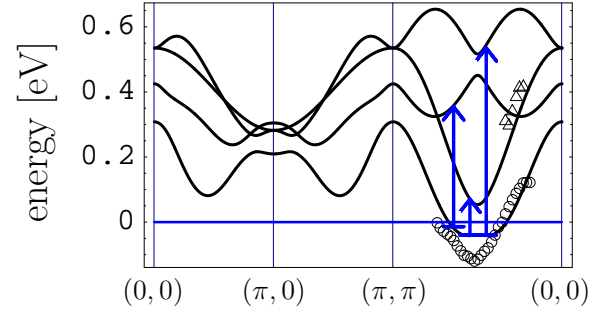


FIG. 5: Band structure obtained by solving the eigenvalue problem (7). Also shown is the dispersion of bands observed by Ronning et al. in $\text{Ca}_2\text{CuO}_2\text{Cl}_2$ [54] (circles and triangles). A sample Fermi level of a doped system has been chosen as the zero of energy. Vertical arrows label possible optical transitions of a hole at the bottom of the band.

the more correct two-band model has been done by Eroles et al. [53].

In a first calculation we want to study the low energy band structure. In the LCAO-like ansatz (6) we first restrict ourselves to the lowest state (i.e. $m = 1$) for each symmetry so that we have to solve 4×4 matrices (we have o_2 ; $p_x, p_y, d_{x^2-y^2}$). The resulting band structure is shown in figure 5. Using the photoemission matrix elements (15) the photoemission spectrum can be calculated, see figure 6. In addition to the familiar quasiparticle band discovered in $\text{Sr}_2\text{CuO}_2\text{Cl}_2$ by Wells et al. [3], which has been discussed extensively in the literature [5, 6, 7, 8, 9, 10, 11, 12, 38, 39] there is a second band with slightly lower intensity which has predominant p -like SP character and runs essentially parallel to the original band. Indeed such a second band with weaker intensity which follows the main band is seen in exact diagonalization of small clusters – see e.g. Figure 1 of Ref [17]. These higher lying SP bands have small spectral weight and therefore could be hard to observe in ARPES – even more so because the ARPES spectra in the undoped compound are likely to show strong lattice polaronic effects [55]. Nevertheless, it may be that a higher lying band – possibly the first p -like band – has been observed by Ronning et al. in the insulating cuprate $\text{Ca}_2\text{CuO}_2\text{Cl}_2$ [54]. There a second weak band has been observed at roughly 0.5 eV below the quasiparticle band. Ronning et al. interpreted this as part of a wide band which reaches ~ 2 eV at a binding energy below 2 eV. As can be seen in Figure 5, however, this band (triangles) has a dispersion that is quite comparable to that of the quasiparticle band (circles). Moreover, as will be discussed below, we believe that the band portion observed in $\text{Ca}_2\text{CuO}_2\text{Cl}_2$ around 2 eV is an example of a ‘1 eV peak’ as observed in $\text{Sr}_2\text{CuO}_2\text{Cl}_2$ [56] and thus unrelated to the band marked by triangles. While the higher lying bands may be hard to observe in ARPES optical interband transitions be-

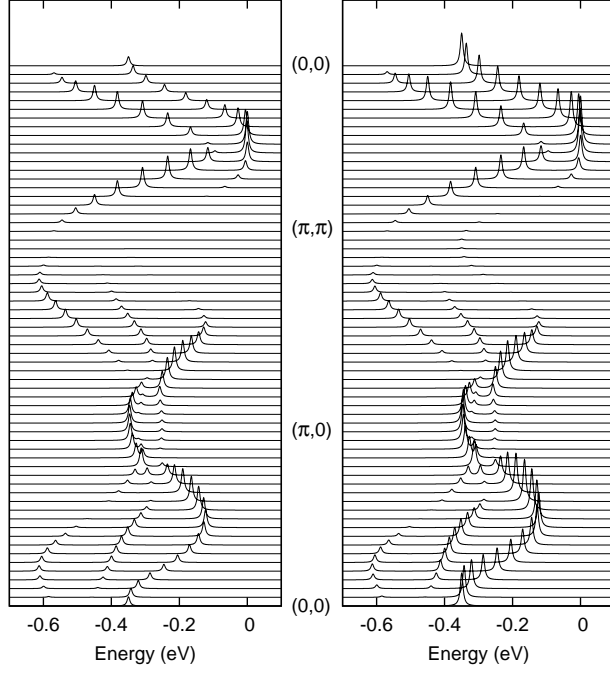


FIG. 6: Photoemission spectrum for the half-filled model corresponding to the band structure (5). In the left panel the spectral weight is computed using only the quantum fluctuation correction (15), in the right panel the charge-fluctuation correction (17) was used as well.

tween the main band and these higher lying bands produce finite-frequency optical conductivity which may correspond to the mid IR bands – again in the actual compounds this may be complicated by polaronic effects. Another feature which can be seen in Figure 6 and which is quite consistent with experiment is the sharp drop of the spectral weight of the quasiparticle band which occurs whenever one passes (roughly) through the Fermi surface of the noninteracting half-filled, i.e. the remnant Fermi surface. It is caused by the k -dependence of the photoemission matrix elements (15) and (17) and therefore reflects the interplay of spin and charge fluctuations in the spin background and the internal structure of the quasiparticle. Assuming that the structure of the quasiparticles remains roughly the same in a spin background without long range order but short ranged antiferromagnetic correlations – as is suggested by exact diagonalization [32] – the k -dependence of the photoemission matrix element should be similar for finite doping. This would provide an immediate explanation for the Fermi arcs seen in the underdoped compounds. To make this more quantitative we have computed the Fermi contour by filling up the single hole dispersion according to the Pauli principle – see Figure 5 – and showed it in the upper panel of Fig. 7. The lower panel shows the spectral weight of the quasiparticle band as a function of the Fermi surface angle. The hole pocket is actually more elongated along the $(1,1)$ direction than along the antiferromagnetic zone boundary. It should be noted, however,

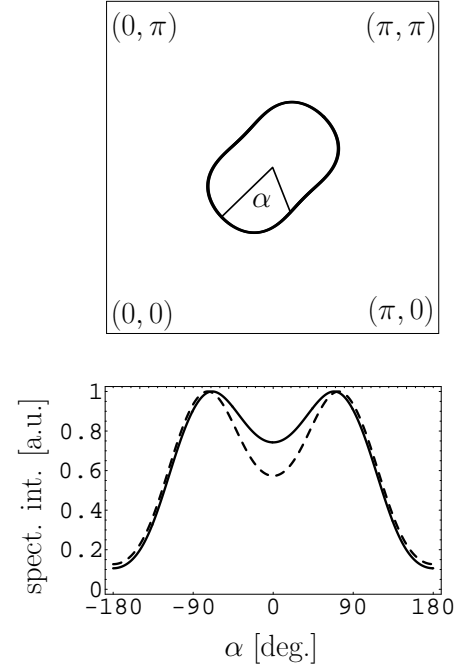


FIG. 7: Top: Fermi surface obtained for 10% hole concentration by rigid filling of the lowest SP-band. Bottom: Spectral weight of the corresponding SP-band along the Fermi surface as a function of the angle α .

that this is calculated at half-filling where $(\pi, 0)$ is far from the valence band top due to the t^0 and t^{π} terms – see Figure 5. On the other hand it is known that upon doping the band portions near $(\pi, 0)$ move upward [13]. It has been suggested that decreasing antiferromagnetic spin correlations lead to an effective downward renormalization of t^0 and t^{π} with doping [17] so that for finite doping the pocket is probably elongated more along the antiferromagnetic zone boundary as observed by Chang et al. [20]. This effect cannot be reproduced by our simple theory, however. Another phenomenon which would need a very simple explanation in an approximate rigid band behaviour upon doping is the pseudogap [13]. The upper part of Figure 8 shows again the hole pocket and a contour in k -space which extends the ‘front part’ of the pocket into a free-electron-like Fermi surface. The pseudogap is usually defined by measuring the leading edge shift or the dispersion of the high-energy feature along such a contour. The lower part of Figure 8 then shows the energy of the quasiparticle band along this ‘Fermi surface’ plotted versus the Fermi surface angle α . There is the characteristic dip at $\alpha = 0$ which originates because the contour initially follows the hole pocket and then the d -wave-like downward dispersion as the free-electron-like Fermi surface departs from the hole pocket. It should be noted that this would explain only the high-energy pseudogap. On the other hand the low-energy pseudogap, being defined in terms of a leading-edge shift,

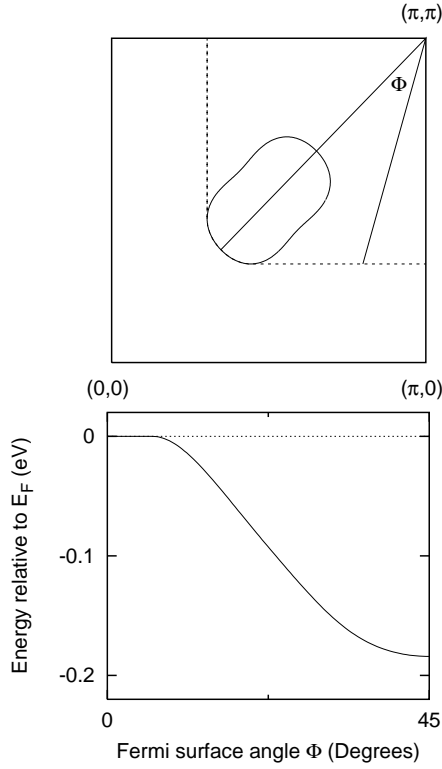


FIG. 8: Top: Fermi surface obtained for 10% hole concentration by rigid fitting of the lowest SP-band and a contour obtained by extending the ‘inner part’ of the pocket to a free-electron-like Fermi surface. Bottom: Energy relative to Fermi energy of the SP band forming the pocket along the free-electron-like Fermi surface as a function of Fermi surface angle.

has no immediate connection with a dispersion relation and will almost certainly depend also on the temperature and momentum dependent linewidth of the quasiparticle band [18]. In fact, assuming a lifetime broadening $\Gamma(k) / \mathcal{E}(k)$ would immediately explain also the low-energy pseudogap. As noted above the pocket in Figure 8 is too much elongated in (1;1)-direction. However, the effective downward renormalization of t^0 and t^{00} in the doped compounds would lead to a pocket that is more elongated along the magnetic zone boundary. In any way, however, if one would go along the inner part of the pocket near (1;1) and extend this to a free-electron-like Fermi surface as in the top part of Figure 8 one will always see a dispersion as shown in the bottom part of Figure 8.

Finally we want to discuss the spectral function on a larger energy scale. To keep the discussion simple we keep only s-like SP states in (6) but include excited s-like states with $m = 1 :: 10$ (extending this to $m = 1 :: 20$ produces no visible change in the spectra – this is one of the beneficial effects of the ‘prediagonalization’ of H_0). Moreover we retain only the matrix elements due to string truncation and the t^0 and t^{00} -terms, i.e. processes

of the type shown in Figure 3. However, we do include the full photoemission matrix elements (15) and (17). The resulting spectral function is shown in Figure 9. In addition to the quasiparticle band – which is essentially identical to the one of the more exact calculation shown in Figure 6 above – there now appear additional bands at higher energy. In reality these bands’ probably are not well-defined states because they are already high in energy. Rather these states are probably strongly broadened due to interaction with magnons and phonons and may have only the character of ‘resonances’. Whereas the quasiparticle band is composed mainly of the lowest s-like SP states for motion of the hole trapped in the linearly ascending potential the higher lying bands correspond to excited levels of the trapped hole. The relatively high intensity of these states may be understood by noting that the coefficients $c_m^{(n)}$ for the excited states $m > 1$ will have extra nodes as functions of Φ and if the signs of the $c_m^{(n)}$ better match the prefactors in (15) the matrix element may even be larger for these higher lying states.

The spectral function in Figure 9 is qualitatively similar to the result of a recent calculation by Bonca et al. [47] which was performed in a string basis with several million basis states. As already noted the main difference between the present calculation and the one by Bonca et al. is in the fact that the ‘prediagonalization’ of H_0 by solution of (4) leads to a quite massive reduction of irrelevant degrees of freedom in the present scheme – as noted above, the matrix diagonalized here is 10×10 . Despite this simplification not only the dispersion of the topmost peak but also the fact that the high energy part ‘widens’ as one moves away from (0;0) is reproduced. On the other hand, it should be also noted that the spectral weight shown in Figure 9 cannot directly be compared with Ref. [47] because we are taking into account the corrections of the ARPES matrix element due to quantum spin fluctuations in the half-filled ground state which are not included there.

V. ELECTRONIC STRUCTURE AT HIGHER BINDING ENERGIES

Recently a number of studies have revealed additional structure in the ARPES spectra at higher binding energies. Ronning et al. found [54] that in the insulating cuprate $\text{Ca}_2\text{CuO}_2\text{Cl}_2$ the quasiparticle band ‘fade away’ as the Γ -point is approached – a phenomenon which is common to all cuprates. The spectral weight that is missing from the quasiparticle band then appears at

1.5 eV below the maximum of the quasiparticle band in the form a high intensity band which has a dispersion that is remarkably consistent with LDA band structure calculations. More precisely this is the antibonding band of $\text{Cu}3d_{x^2-y^2}$ and $\text{O}2p$ orbitals – whereby it has to be kept in mind that at these two orbitals do not hybridize due to parity, so that in an LCAO-like description these

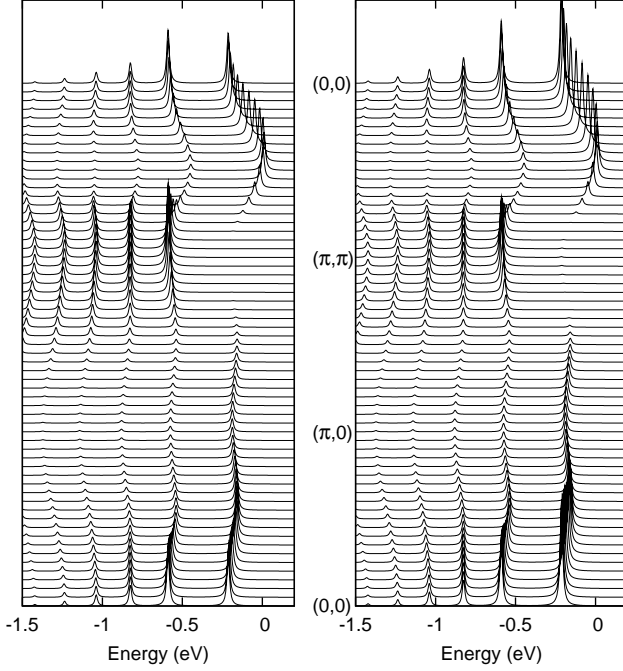


FIG. 9: Spectral density for hole creation at half-filling along high-symmetry lines in the Brillouin zone. Calculated with (right) and without (left) the contribution from charge fluctuations.

bands have pure oxygen character at Γ and π -by continuity in k - very small Cu3d admixture in its neighborhood.

Similar behaviour was observed in doped cuprates as well [57, 58, 59, 60, 61]. In addition, the so-called waterfall-phenomenon is observed. Moving e.g. along the $(1;1)$ direction towards π the quasiparticle band first disperses away from the Fermi edge but then - at a momentum of approximately $(\frac{\pi}{2}; \frac{\pi}{2})$ - seems to bend down sharply and drop almost vertically down to an energy of 1 eV below the Fermi edge. The apparent vertical part of the dispersion - the 'waterfalls' - can be seen as a hump in momentum distribution curves at binding energies in the range of 0.5 eV - 1.0 eV. Upon reaching 1 eV below E_F the vertical parts then merge with two LDA-like bands of high intensity.

Similar behaviour - namely small band portions with a free electron-like dispersion and high spectral weight near high symmetry points of the Brillouin zone - has been observed previously in the insulating compound $\text{Sr}_2\text{CuO}_2\text{Cl}_2$ by Pothuizen et al. [56]. The interpretation given by these authors was that these are O 2p derived states which do not hybridize with Cu3d orbitals due to symmetry - which is why they appear only at high-symmetry points of the Brillouin zone - and hence are unaffected by the strong correlations in the partially filled Cu3d orbitals. This explains their LDA-like dispersion and high spectral weight because they are essentially free electron states.

We believe that an important clue to the interpretation of the waterfalls is the finding of Inosov et al. who

showed that matrix element effects play a crucial role in their observation [62] and that the missing part of the quasiparticle band near π can in fact be observed with photon energies around 100 eV where the cross section for Cu3d orbitals becomes appreciable [63]. Moreover, Pan et al. found that the waterfalls show the same dependence on photon polarization as the quasiparticle band itself, indicating that they also are derived from Zhang-Rice singlets [60]. And finally in our opinion the crucial clue is the fact, that the quasiparticle band itself cannot be observed near the Γ -point either. While numerical studies of the Hubbard and t-J model [64, 65, 66] - as well as the present theory - do indeed predict that the spectral weight of this band is lower by a factor of 2-3 at Γ as compared to $(\frac{\pi}{2}; \frac{\pi}{2})$, in experiment there is practically no more intensity visible. Rather, the spectra show a complete suppression of spectral weight around Γ which extends down to the intense LDA-like bands. Most significantly, however, the waterfalls appear at very nearly the same momentum where the quasiparticle band itself becomes visible.

We conclude that the reason for the vanishing of the quasiparticle band near Γ is 'extrinsic' to the t-J or single-band Hubbard model namely the special combination of phases for the O 2p orbitals in the bonding combination which hybridizes with a given Cu3d_{x²-y²} orbital in the Zhang-Rice singlet (ZRS). In the framework of a simple three-step model of photoemission for photoemission the effect that we seek comes from the matrix element for the dipole transition from O 2p states into the final state - which we take to be a plane wave with momentum k for simplicity. For definiteness we introduce the dipole matrix element

$$v = \frac{1}{V} \int d\mathbf{r} e^{i\mathbf{k} \cdot \mathbf{r}} \mathbf{r} \cdot \langle \mathbf{r} | \quad (18)$$

where \mathbf{v} denotes the polarization vector of the light, V the volume of the crystal, $\langle \mathbf{r} |$ is the wave function of an O 2p orbital at the origin and $\mathbf{r} = x\mathbf{e}_x + y\mathbf{e}_y$. The matrix element for a dipole transition from the bonding combination of O 2p oxygen orbitals around a given Cu site j

$$P_j = \frac{1}{2} (p_{j+\frac{x}{2}}; p_{j-\frac{x}{2}}; p_{j+\frac{y}{2}} + p_{j-\frac{y}{2}}) \quad (19)$$

into the plane wave state is

$$m_{ZRS} = e^{i\mathbf{k} \cdot \mathbf{R}_j} i v_y \sin \frac{k_y}{2} v_x \sin \frac{k_x}{2} : \quad (20)$$

Note that the k dependence of the expression in square brackets comes solely from the interplay between the phase factors $e^{i\mathbf{k} \cdot \mathbf{r}}$ on the four oxygen neighbors of atom j and the relative phases of the orbitals in (19). Namely any two oxygen orbitals whose position in real space differ by one lattice spacing have a relative phase of (-1) in the ZRS - which would correspond to momentum $(\frac{\pi}{2}; \frac{\pi}{2})$. This k dependence is therefore completely independent

of details in the computation of the matrix elements v and therefore in particular independent of the photon polarization. Moreover it would stay the same if a more realistic state wave function were used as long as this is a Bloch state with momentum k . It now can be seen that $m_{ZRS} \neq 0$ as $k \neq (2n; 2m)$. Unlike the argument based on the dipole selection rule which was discussed by Ronning et al. [54] the expression (20) thus explains why the quasiparticle band has vanishing intensity not only at Γ but at all equivalent points in higher Brillouin zones as well.

The above considerations apply only to hole creation on oxygen. For photon energies around 20 eV it is well known, however, that the cross section for hole creation on oxygen is considerably larger than for hole creation in transition metal 3d orbitals [63]. Moreover, starting from a d^9 state one would reach a d^8 state. The latter is high in energy and hence has small weight in the ZRS and moreover the resulting spectral weight would be spread over several eV due to the multiplet splitting of d^8 so that the corresponding matrix element certainly is small. A d^9 final state could be produced by photoemission from d^{10} state but this state also is high in energy and therefore has small weight in the ground state. In any way the contribution of hole creation on Cu is strongly suppressed. For larger photon energies – around 100 eV – Inosov et al. could indeed resolve the quasiparticle band [62] but only at $(2; 0)$. Obviously the larger photoemission cross section and the non-validity of the dipole selection rule at this momentum make it possible to see intensity from photoholes in $Cu 3d_{x^2-y^2}$ orbitals. Clear evidence that the intensity seen there is due to photohole creation on Cu is also provided by the strong variation of intensity around the $Cu 3p \rightarrow Cu 3d$ threshold which is being used routinely to identify transition metal 3d states in other transition metal oxides [67].

One might then ask, where the spectral weight corresponding to hole creation on oxygen goes at Γ . The answer is that this spectral weight is concentrated in the LDA-like bands which are observed around the Γ -point at approximately 1.5 eV below the Fermi energy. Due to parity the ‘antibonding band’ of $Cu 3d_{x^2-y^2}$ and $O 2p$ orbitals actually has pure oxygen character at Γ . If a Bloch state of $O 2p$ orbitals is created with momentum $(0; 0)$ this cannot couple to the ZRS singlet – see (20) – but has overlap with these bandlike states. This is the same reasoning as given by Pothuizen et al. [56] for the ‘1 eV peaks’ in $Si_2CuO_2Cl_2$. The spectral weight transfer from the quasiparticle band to the ‘1 eV peaks’ at Γ as observed by Ronning et al. thus is strong evidence for the ZRS-character of the quasiparticle band.

This leaves the question as to what is the interpretation of the waterfalls. The above considerations suggest that these are simply the higher lying SP bands seen in Figure 9. These bands are likely to be strongly broadened due to interaction with spin excitations and possibly also phonons although one of them may have been resolved by Ronning et al. [54] (see Figure 5). Near the spec-

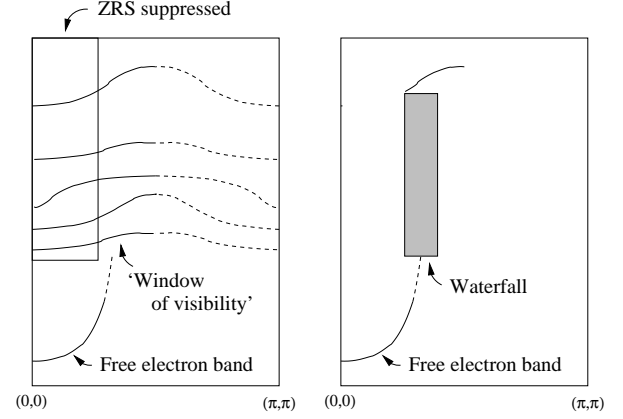


FIG. 10: Interpretation of the waterfall phenomenon. A round photohole on oxygen do not couple to the ZRS whence all t - J derived states have no spectral weight. Photoholes created with this momentum on oxygen instead propagate as (nearly) free-electron states which do not hybridize with the correlated Cu d -orbitals. Moving away from the t - J bands become visible but lose spectral weight as well (dashed portions). The nearly free-electron states cease to exist because they now have appreciable hybridization with the correlated Cu d -orbitals. The higher lying SP bands thus are visible only in a small window in k -space i.e. the waterfalls.

tral weight of these bands disappears because they are also ‘ t - J -derived’ and the matrix element for creation of a ZRS vanishes see Figure 10. As one moves away from the matrix element for creation of a ZRS increases but – as can be seen in Figure 9 – the spectral weight of these excited SP bands now quickly decreases. It follows that the spectral weight of these bands must go through a maximum as one moves away from Γ and this is our interpretation of the ‘waterfalls’: a number of essentially incoherent states which have a ‘window of visibility’ in a narrow range of momenta around $(\frac{\pi}{4}; \frac{\pi}{4})$ and this window of visibility is seen as the hump in the momentum distribution curves. Since the suppression of these states near Γ is governed by the same matrix element of the ZRS as the quasiparticle band itself, it is moreover clear that this window of visibility ‘opens’ precisely in the same range of k where the quasiparticle band itself becomes visible – hence the apparent downward bending and the waterfall-like appearance of the spectra.

A more quantitative description of this phenomenon obviously would have to start out from a three-band model so as to describe both, the coupling of a photohole to a ZRS and the existence of the nearly free electron states at high-symmetry points. This is out of the scope of the present paper and we therefore make no attempt for a quantitative discussion. There have been a number of attempts to explain the waterfall phenomenon within the t - J model [51, 68]. However, as was already noted,

the experimental spectra show a complete suppression of spectral weight around which extends downward all the way to the intense LDA-like bands. This behaviour is not reproduced by t-J model calculations which show spectral weight – corresponding to the higher lying bands in Figure 9 – at too low binding energy. Moreover, the LDA-like dispersion of the high-intensity parts near is not really reproduced

VI. OPTICAL CONDUCTIVITY

Finally we turn to a discussion of the optical conductivity thereby using the results of the simplified calculation which took into account only the lowest ($m = 1$) state for each symmetry ϕ . As is the case for atomic wave functions the s and d-like SP states on one hand and the p-like SP states on the other have opposite parity and hence can have nonvanishing matrix elements of the current operator in between them. If we assume again that the quasiparticle band is filled with holes upon doping – which would occupy momenta around $(\frac{\pi}{2}; \frac{\pi}{2})$ – we thus expect optical interband transitions (as indicated in Figure 5) which should be observable in the finite frequency optical response. This is defined as

$$\langle q = 0; ! \rangle = \sum_{n \neq 0} \frac{1}{i} \langle \mathbf{j}_n \rangle \langle q = 0 \rangle \langle j_0 | i^2 \rangle$$

$$(! = (E_n - E_0)):$$

where j_n (E_n) denotes the n -th eigenstate (eigenenergy) of the system (in particular, $n = 0$ denotes the ground state). Also, j , with $= x; y$ denotes a component of the current operator,

$$j(q) = i \sum_{m,n} t_{mn} e^{iq(R_m + R_n) \cdot 2} [R_m - R_n] \cdot \hat{c}_m^\dagger \hat{c}_n; \quad (21)$$

Assuming a filling of the quasiparticle band we approximate this by

$$(!) = 2 \sum_{k, l=1}^X \sum_{l=1}^X \frac{1}{i} \langle \mathbf{j}_1(k) \rangle \langle \mathbf{j}_1(k) | i^2 n_k \rangle$$

$$(! = (E_1(k) - E_1(k))) : \quad (22)$$

where n_k denotes the hole occupation of the quasiparticle ($l = 1$) band. To evaluate this we need matrix elements of the current operator between the localized SP states (2): $\langle \mathbf{j}_i \rangle \langle \mathbf{j}_i^0 \rangle$ (with $= (0; m)$). The main contribution to this matrix element are shown in Figure 11. Starting from a bare hole – the ‘string of length 0’ – the current operator j_y generates two strings of length 1 but with opposite sign. These two string states thus have precisely the right sign to couple to a p_y -like SP state, see the sign convention in Figure 2. From this and similar processes we obtain the matrix element

$$\langle \mathbf{j}_i^{(p;0)} \rangle \langle \mathbf{j}_i^{(s;0)} \rangle = 2i \left(\sum_{=0}^X \mathbf{0}_{+1} - \sum_{=1}^X \mathbf{0}_{+1} \right) : \quad (23)$$

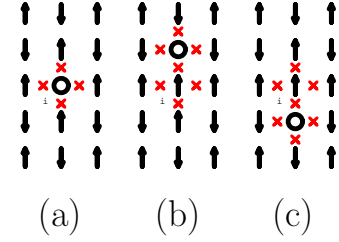


FIG. 11: Application of the current operator j_y to a bare hole in the Neel state (a) creates two strings of length 1 (b) and (c) with opposite signs.

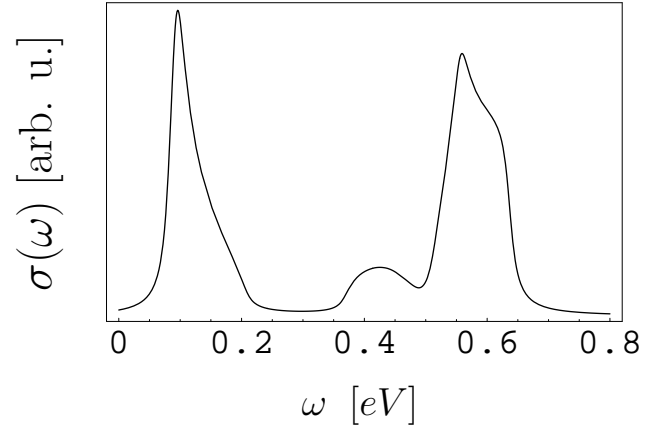


FIG. 12: Optical conductivity at 10% hole concentration.

All matrix elements generated in a similar way and involving SPs of different symmetries or hopping at longer distances have been listed in the Appendix B. The resulting optical conductivity at a hole concentration of 10% is shown in Figure 12. While the higher lying bands with p-character have small spectral weight and hence are difficult to observe in ARPES, they dominate the optical conductivity. We note that the present interpretation of the optical conductivity is consistent with that of Ref. [43] and [34]. One may expect that the excited levels of the trapped hole – or ‘internal degrees of freedom’ of the SP quasiparticles – are also seen in the dynamical density correlation function. Vojta and Becker [34] have calculated the dynamical density correlation function in a string framework similar to the one used by Bonci et al. and obtained convincing agreement with exact diagonalization results. Within our approach one can naturally explain the distribution and spreading of the spectral intensity over a wide energy range, which has been observed in experiments [69, 70]. Due to the Brillouin folding in the AF state the center of the hole pocket at $(\pi/2; \pi/2)$ is a high symmetry point. s, d, and p SP states do not mix with each other exactly at this point. Thus, the transitions with similar intensity occur in the weakly doped system between the lowest predominantly s-like

and the first and the third predominantly p-like bands. Wider spreading of the high intensity region at higher energies can be attributed to the admixture of p-wave SPs to the lowest band and transition to the predominantly d-wave second excited band.

VII. DISCUSSION AND CONCLUSIONS

In summary we have presented a theory for spin polaron-like quasiparticles. The basic idea is that a hole in an antiferromagnetically ordered 'spin background' is self-trapped which actually requires only short-range antiferromagnetic order. This will lead to a hierarchy of localized states which may also realize different irreducible representations of C_{4v} . Since the Heisenberg exchange and the t^0 and t^{00} terms have matrix elements between such self-trapped states on neighboring sites an LCAO-like description emerges where the role of the atomic or Wannier functions is played by the levels of the self-trapped hole. This leads to a multi band structure for the doped holes with the lowest of these being the familiar quasiparticle band observed in the insulating compounds and discussed extensively in the literature. Here we take the point of view that the simplest description for the underdoped compounds is holes being filled into this quasiparticle band. The fact that these self-trapped states extend over several unit cells in real space necessarily implies that they have an ARPES form factor which varies within the first Brillouin zone - hence the strong variation of the photoemission intensity of the quasiparticle band as a function of k which explains the remnant Fermi surface and the Fermi arcs seen in ARPES. Moreover, the pseudogap becomes a triviality within this picture. One of the higher bands of the effective LCAO-Hamiltonian may have been observed in ARPES in the insulator $\text{Ca}_2\text{CuO}_2\text{Cl}_2$ and optical transitions between the resulting bands may explain the mid-infrared band in optical spectroscopy. There are probably complications due to lattice polaron effects but here we neglect these although the simplicity of the present calculation - which never needs matrices to more than 10×10 - would certainly allow to treat such effects as well.

The main drawback of the present theory is the use of a spin background with antiferromagnetic order - which clearly is not realized in doped materials of interest. On the other hand all processes by which the hole propagates involve only spins in its immediate neighborhood. One may therefore expect that very similar processes would occur in a spin background with only short range antiferromagnetic correlations so that much of the present theory should apply in this case as well. The most important effect we are missing with the present calculation is the closing of the pseudogap with both increasing temperature and increasing doping. Since this closing implies that the dispersion actually approaches that for the 'pure' t - J model - i.e. without t^0 and t^{00} terms - this effect could be described by an effective downward renormalization of

the t^0 and t^{00} terms. The mechanism may be the decrease of spin correlations: in the Neel state the t^0 and t^{00} terms can transport a hole 'completely coherent' i.e. without creating a spin excitation. As the spin correlation length decreases and reaches the 'range' of these terms in real space - two lattice spacings - the t^0 and t^{00} will increasingly generate spin excitations when transporting a hole so that they change their net effect from coherent hole transport to 'excitation generating' hole transport.

Acknowledgments

P.W. acknowledges encouragement and valuable comments from P. Fulde and R. Micnas. He also appreciates discussions with M. Jarrel, P. P. Relovsek, and T. Tohyama.

APPENDIX A: SPIN POLARON MODEL

We first derive the equations for the coefficients (ϕ_m) in (2), thereby assuming (3). We denote by j the sum of all string states with inverted spins, each multiplied by the proper phase factors according to figure 2. On a Bethe lattice the number of such states is $n = f^{(o)} z(z-1)^{l-1}$ where $f^{(o)} = 1$ for $o = s; d_{x^2-y^2}$ and $f^{(o)} = 1/2$ for $o = p_x; p_y$. Our normalized basis states are $j = n^{1/2} |j\rangle$ which obey

$$h + 1 |j\rangle = t \frac{r}{n+1} |j\rangle$$

because each of the $n+1$ basis string states in the bra is generated exactly once from a state in the ket and the matrix element for hopping of a hole is positive. The states (2) can be written as

$$|j\rangle = \sum_i |i\rangle$$

with $|i\rangle = n^{1/2} (\phi_m)$. Performing the variational procedure - thereby using (1) - we obtain the set of equations

$$E_0 \phi_0 + \frac{p}{z} \phi_1 = E_0 \phi_0 \quad (A1)$$

$$E_1 \phi_1 + \frac{p}{z} \phi_0 + \frac{p}{z} \phi_2 = E_1 \phi_1 \quad (A2)$$

$$E_0 \phi_0 + \frac{p}{z} \phi_1 + \frac{p}{z} \phi_2 = E_0 \phi_0 \quad (A3)$$

For $o = p_x; p_y; d_{x^2-y^2}$ one has to set $\phi_0 = 0$ and discard the first equation. After introducing a cutoff for these equations can be solved numerically.

Now we proceed to analyse with some sample processes which give rise to nonvanishing matrix elements (10) and (11). The hopping integral t is the highest energy scale among all model parameters t, t^0, t^{00} , and J . On the other hand, the exchange energy grows fast with the number of fluctuations. That number is directly related to the length of paths P_i . This mechanism is responsible for the

tendency towards hole confinement and the construction of SPs also relies on it. Quasiparticle deconfinement occurs due to processes which are mediated by hopping to second and third NN and by the action of the XY term in the exchange interaction. Only string states \mathcal{P}_{ji} with a low number of fluctuations can be involved in those processes at the low energy scale. Thus, in order to find matrix elements (10) we need to determine coupling between short-string states \mathcal{P}_{ji} . That coupling is induced by the perturbation part H_1 which by definition contains terms related to hopping to second and third NN sites and which also contains the XY term. We restrict our considerations to processes involving string states \mathcal{P}_{ji} which are related to paths not longer than 2 lattice spacings for s-wave SPs and to paths not longer than 3 lattice spacings for SPs with lower symmetry. In the latter case we take into account longer strings because the zero-length string state \mathcal{P}_{ji} does not contribute to the wavefunction (2) of SPs with lower symmetry and thus the weight is shifted to states representing longer paths. The absolute values of prefactors $t_0^{(1)}$ corresponding to lowest eigenstates of (A1)–(A3) rapidly decrease with the string length which additionally justifies the restriction of our considerations to strings with short length. At the level of the approximation which we apply, there exist more than 20 categories of processes which contribute to (10) and (11). The differences between different categories concern the underlying mechanisms or the geometry of involved strings. Since the mechanisms which give rise to coupling between s-wave SPs were discussed in detail in the past [40, 44] here we will mainly concentrate on the issue how the lowering of SP symmetry influences the coupling between SPs and we will discuss representative examples of processes which give rise to the hybridization between SPs. In order to keep the Hilbert space as small as possible we consider at first the low energy sector and analyze only lowest SP states with given symmetry.

For example, Fig. 13 (a), (b) depicts a process during which a SP polaron is shifted to a second NN site. (a) represents a string state \mathcal{P}_{ji} which is a component of the wavefunction (2) of a SP created at site i . This state has been obtained by creating a bare hole in the Neel state. It appears with the prefactor $t_0^{(1)}$ in the superposition (2) defining the s-wave SP at site i . With the same prefactor appears the string state depicted in Fig. 13 (b). It is a component of the s-wave SP created at site j . Since string states (a) and (b) are coupled by the second NN hopping term a non-vanishing matrix element (10) between s-wave SPs is generated. The related contribution to that matrix element is given by

$$T_{ji}^{((s;0)(s;0))} T_{R_j R_i}^{(ss)} = T_{ss}^{(1)} = t_0^{(1)} \quad (A4)$$

Within a convention for presenting matrix elements this contribution can be written as

$$ss; \hat{x} + \hat{y}; \begin{pmatrix} 1 \\ ss \end{pmatrix} : C_4 : \quad (A5)$$

The presence of the group symbol C_4 in (A5) means that additional contributions to (10) can be obtained by apply-

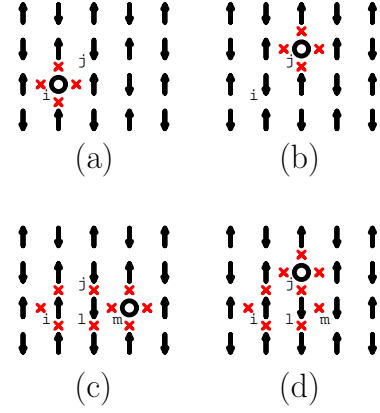


FIG. 13: (Color online) (a) and (b) A process which gives rise to the shift of the s-wave SP to a second NN site. (c) and (d) A process which generates corrections to eigenenergies E_1 and E_1^0 of SPs.

ing to (A4) elements of C_4 different than identity. Since $t_0^{(1)} = 0$ states depicted in Fig. 13 (a) and (b) do not contribute to SP wavefunctions (2) with lower symmetry. Thus the above discussed lowest-order process does not generate hybridization in which such SPs are involved. By process order we understand, in terms of the conventional perturbation theory, the total number of Hamiltonian actions necessary to transform a state representing a bare hole created in the AF background into another such state. It is clear that this parameter is related to the sum of lengths for paths involved in a given process.

The origin of the formula for the integral $t_{ss}^{(1)}$ in (A4) is rather obvious. It is the product of prefactors which appear by string states depicted in Fig. 13 (a) and (b) in the definition for the wavefunctions of SPs at sites i and j . $t_0^{(1)}$ is the integral which appears as a prefactor in the hopping term coupling those string states. The same scheme can be applied to deduce the form of hopping integrals which appear in further terms in $T_R^{(00^0)}$.

Fig. 13 (c) and (d) depicts a process which gives rise to corrections to SP eigenenergies E_1 and E_1^0 of SPs and amendments to the diagonal term in (8). Those corrections originate with the coupling between different string states generated by the hopping to second NN sites. Those string states contribute to the wavefunctions of SPs created at the site i . The paths \mathcal{P}_i corresponding to string states \mathcal{P}_i depicted in Fig. 13 (b), (c) have been shown in Fig. 14 (a), (b), respectively. From now on we will also use the latter form of diagrams to represent string states. The same mechanism as discussed above works for pairs of longer strings which have identical form with the exception of hole positions at ends of them. The corrections to energies of s-wave d-wave and p-wave SPs are $t_{ss}^{(13)}$, $t_{dd}^{(13)}$ and $t_{pp}^{(13)}$ respectively. Their explicit form can be found below. Due to point-group properties the above discussed process does not generate the coupling between SPs with different symmetries.

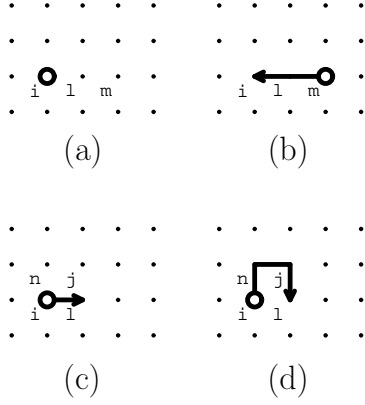


FIG. 15: (a) and (b) A low-order process which involves the action of the transverse part of the exchange term and gives rise to the hybridization of SPs with different symmetry. (c) and (d) String states involved in a process mediated by the XY part of the exchange term and resulting in a correction to the eigenenergy of the d-wave SP.

third NN site are given by $_{ss}^{(3)}$, $_{ds}^{(3)}$, and $_{ps}^{(3)}$ respectively.

A similar mechanism gives rise to a correction to the eigenenergy of a d-wave SP. The action of the XY term flips spins in the string state depicted in Fig. 15 (c) at sites n , j and creates the string state shown in Fig. 15 (d). Due to the fact that both string states contribute to the wavefunctions (2) of SPs created at the same site i and due to standard selection rules, the contribution to $T_R^{(oo^0)}$ originating with the above discussed process must be diagonal. For this reason, p-wave states can not contribute to the related new matrix elements $T_R^{(oo^0)}$, because the process depicted in Fig. 15 (c), (d) involves string states which contribute to different p_x-wave and p_y-wave SPs. Since the length of the string depicted in Fig. 15 (d) is 3 lattice spacings we neglect the correction to the eigenenergy of the s-wave SP, because we expect that it is small. The correction to the eigenenergy of the d-wave SP is $_{dd}^{(11)}$. It also contains contributions related to the coupling, in the same way, between longer-string states obtained by letting holes at the ends of strings in Fig. 15 (c) and (d) to hop further along identical paths.

During the construction of SPs we have been assuming that wavefunctions of SPs at different sites are orthogonal which turns out not to be an exactly true assumption. On the other hand the overlap between SPs is rather small because it originates with the overlap of nominally different string states related with paths of relatively long length. Such string states have been depicted in Fig. 16 (a) and (b). Both Figures 16 (a) and (b) actually represent the same state which consists of a hole at site j and fluctuations at sites n , i , l created in the Neel state. The generated in this way overlap between different SPs also

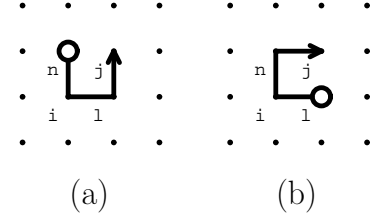


FIG. 16: (a) and (b) Spuriously different string states which are actually identical, what gives rise to the overlap between SPs created at sites n and l .

gives rise to a new contribution in the Hamilton operator,

$$p_y d; \hat{x} + \hat{y}; E_1^{(1)} \big|_{pd} : C_{4v} \quad H \mathcal{C} : \quad (A 8)$$

$$dd; \hat{x} + \hat{y}; E_1^{(1)} \big|_{dd} ; p_y p_x; \hat{x} + \hat{y}; E_1^{(1)} \big|_{pp} : C_{4v} : (A 9)$$

The analysis of other processes which give rise to new elements of $T_R^{(oo^0)}$ is rather straightforward and similar to the analysis of previously discussed processes. Thus we do not discuss the remaining contributions to $T_R^{(oo^0)}$ one by one.

Finally, we list here matrix matrix elements which determine the form of the Hamilton matrix (8), (10),

$$ss; 0; E_1; dd; 0; E_1^{(1)}; p_x p_x; 0; E_1^{(1)}; p_y p_y; 0; E_1^{(1)} : (A 10)$$

$$ss; 0; \big|_{ss}^{(6)}; ss; \hat{x} + \hat{y}; \big|_{ss}^{(1)}; ss; 2\hat{x}; \big|_{ss}^{(2;0)};$$

$$dd; 0; \big|_{dd}^{(6)}; dd; 2\hat{x}; \big|_{dd}^{(14)}; p_x p_x; 0; \big|_{pp}^{(6)};$$

$$p_x p_x; 2\hat{x}; \big|_{pp}^{(14)} : C_4 \quad (A 11)$$

$$ss; 0; \big|_{ss}^{(13)}; ss; 2\hat{x}; \big|_{ss}^{(3)}; ds; 2\hat{x}; \big|_{ds}^{(2;0)};$$

$$dd; 0; \big|_{dd}^{(13)}; dd; 2\hat{x}; \big|_{dd}^{(7)}; dp_x; 2\hat{x}; \big|_{dp}^{(7)};$$

$$p_x s; 2\hat{x}; \big|_{p_x s}^{(2;0)}; p_x d; 2\hat{x}; \big|_{p_x d}^{(2;0)};$$

$$p_x p_x; 0; \big|_{pp}^{(13)}; p_x p_x; 2\hat{x}; \big|_{pp}^{(7)} : C_4 \quad H \mathcal{C} : \quad (A 12)$$

$$ss; \hat{x} + \hat{y}; \big|_{ss}^{(3)}; sd; \hat{x} + \hat{y}; \big|_{sd}^{(21)};$$

$$sp_x; \hat{x} + \hat{y}; \big|_{sp}^{(21)}; dd; \hat{x} + \hat{y}; \big|_{dd}^{(1;1)};$$

$$dd; 0; \big|_{dd}^{(11)}; dd; 2\hat{x}; \big|_{dd}^{(7)};$$

$$dp_x; \hat{x} + \hat{y}; \big|_{dp_x}^{(1;1)}; p_x d; \hat{x} + \hat{y}; \big|_{p_x d}^{(1;1)};$$

$$p_x d; 2\hat{x}; \big|_{pd}^{(7)}; p_x p_x; \hat{x} + \hat{y}; \big|_{p_x p_x}^{(1;1)};$$

$$p_y s; \hat{x} + \hat{y}; \big|_{p_y s}^{(1;1)}; p_y d; \hat{x} + \hat{y}; \big|_{p_y d}^{(1;1)};$$

$$p_y p_x; \hat{x} + \hat{y}; \big|_{p_y p_x}^{(1;1)} : C_{4v} \quad H \mathcal{C} : \quad (A 13)$$

$$ss; 0; \big|_{ss}^{(0;0)}; ss; \hat{x} + \hat{y}; \big|_{ss}^{(15)};$$

$$dd; 0; \big|_{dd}^{(0;0)}; dd; \hat{x} + \hat{y}; \big|_{dd}^{(1;1)};$$

$$p_x p_x; 0; \big|_{p_x p_x}^{(0;0)}; p_x p_x; \hat{x} + \hat{y}; \big|_{pp}^{(23)};$$

$$p_y p_x; \hat{x} + \hat{y}; \big|_{p_y p_x}^{(1;1)} : C_{4v} \quad (A 14)$$

$$p_y p_x; \hat{x} + \hat{y}; \big|_{pp}^{(21)} : C_{2v} \quad H \mathcal{C} : \quad (A 15)$$

and of the overlap matrix (9), (11),

$$p_y d; \hat{x} + \hat{y}; !_{pd}^{(1)} : C_{4v} \quad H \quad C : \quad (A16)$$

$$dd; \hat{x} + \hat{y}; !_{dd}^{(1)} ; p_y p_x; \hat{x} + \hat{y}; !_{pp}^{(1)} : C_{4v} : (A17)$$

where

$$\begin{pmatrix} \cdot \\ ss; (2;0) \end{pmatrix} = \begin{pmatrix} 2 \\ ss \end{pmatrix} + \begin{pmatrix} 14 \\ ss \end{pmatrix}; \quad (A18)$$

$$\begin{pmatrix} \cdot \\ ds; (2;0) \end{pmatrix} = \begin{pmatrix} 3 \\ ds \end{pmatrix} + \begin{pmatrix} 14 \\ ds \end{pmatrix}; \quad (A19)$$

$$\begin{pmatrix} \cdot \\ p_x s; (2;0) \end{pmatrix} = \begin{pmatrix} 3 \\ ps \end{pmatrix} + \begin{pmatrix} 14 \\ ps \end{pmatrix}; \quad (A20)$$

$$\begin{pmatrix} \cdot \\ p_x d; (2;0) \end{pmatrix} = \begin{pmatrix} 7 \\ pd \end{pmatrix} + \begin{pmatrix} 14 \\ pd \end{pmatrix}; \quad (A21)$$

$$\begin{pmatrix} \cdot \\ dd; (1;1) \end{pmatrix} = \begin{pmatrix} 11 \\ dd \end{pmatrix} + \begin{pmatrix} 17 \\ dd \end{pmatrix} + \begin{pmatrix} 18 \\ dd \end{pmatrix}; \quad (A22)$$

$$\begin{pmatrix} \cdot \\ dp_x; (1;1) \end{pmatrix} = \begin{pmatrix} 7 \\ pd \end{pmatrix} + \begin{pmatrix} 11 \\ pd \end{pmatrix} + \begin{pmatrix} 17 \\ pd \end{pmatrix} + \begin{pmatrix} 18 \\ pd \end{pmatrix}; \quad (A23)$$

$$\begin{pmatrix} \cdot \\ p_x d; (1;1) \end{pmatrix} = \begin{pmatrix} 7 \\ pd \end{pmatrix} + \begin{pmatrix} 11 \\ pd \end{pmatrix} + \begin{pmatrix} 23 \\ pd \end{pmatrix}; \quad (A24)$$

$$\begin{pmatrix} \cdot \\ p_x p_x; (1;1) \end{pmatrix} = \begin{pmatrix} 7 \\ pp \end{pmatrix} + \begin{pmatrix} 11 \\ pp \end{pmatrix}; \quad (A25)$$

$$\begin{pmatrix} \cdot \\ p_y s; (1;1) \end{pmatrix} = \begin{pmatrix} 3 \\ ps \end{pmatrix} + \begin{pmatrix} 15 \\ ps \end{pmatrix}; \quad (A26)$$

$$\begin{pmatrix} \cdot \\ p_y d; (1;1) \end{pmatrix} = \begin{pmatrix} 7 \\ pd \end{pmatrix} + \begin{pmatrix} 15 \\ pd \end{pmatrix} + \begin{pmatrix} 17 \\ pd \end{pmatrix} + \begin{pmatrix} 18 \\ pd \end{pmatrix}$$

$$+ \begin{pmatrix} 0 \\ E_1 \quad J=2 \end{pmatrix} !_{pd}^{(1)} + \begin{pmatrix} 21 \\ pd \end{pmatrix}; \quad (A27)$$

$$\begin{pmatrix} \cdot \\ p_y p_x; (1;1) \end{pmatrix} = \begin{pmatrix} 7 \\ pp \end{pmatrix} + \begin{pmatrix} 17 \\ pp \end{pmatrix} + \begin{pmatrix} 18 \\ pp \end{pmatrix}; \quad (A28)$$

$$\begin{pmatrix} \cdot \\ ss; (0;0) \end{pmatrix} = \begin{pmatrix} 5 \\ ss \end{pmatrix} + \begin{pmatrix} 16 \\ ss \end{pmatrix}; \quad (A29)$$

$$\begin{pmatrix} \cdot \\ dd; (0;0) \end{pmatrix} = \begin{pmatrix} 5 \\ dd \end{pmatrix} + \begin{pmatrix} 16 \\ dd \end{pmatrix} + \begin{pmatrix} 19 \\ dd \end{pmatrix} + \begin{pmatrix} 22 \\ dd \end{pmatrix}; \quad (A30)$$

$$\begin{pmatrix} \cdot \\ dd; (1;1) \end{pmatrix} = \begin{pmatrix} 15 \\ dd \end{pmatrix} + \begin{pmatrix} 0 \\ E_1 \quad J=2 \end{pmatrix} !_{dd}^{(1)} + \begin{pmatrix} 21 \\ dd \end{pmatrix} \quad (A31)$$

$$\begin{pmatrix} \cdot \\ p_x p_x; (0;0) \end{pmatrix} = \begin{pmatrix} 16 \\ pp \end{pmatrix} + \begin{pmatrix} 19 \\ pp \end{pmatrix}; \quad (A32)$$

$$\begin{pmatrix} \cdot \\ p_y p_x; (1;1) \end{pmatrix} = \begin{pmatrix} 15 \\ pp \end{pmatrix} + \begin{pmatrix} 0 \\ E_1 \quad J=2 \end{pmatrix} !_{pp}^{(1)}; \quad (A33)$$

$$\begin{pmatrix} 1 \\ ss \end{pmatrix} = t_{00}^0; \quad (A34)$$

$$\begin{pmatrix} 2 \\ ss \end{pmatrix} = t_{00}^0; \quad (A35)$$

$$\begin{pmatrix} 3 \\ ss \end{pmatrix} = \frac{J}{2} X_{=0}^3 + 2; \quad (A36)$$

$$\begin{pmatrix} 3 \\ ds \end{pmatrix} = \frac{J}{4} X_{=0}^3 + 2; \quad (A37)$$

$$\begin{pmatrix} 3 \\ ps \end{pmatrix} = \frac{J}{2} X_{=0}^3 + 2; \quad (A38)$$

$$\begin{pmatrix} 5 \\ ss \end{pmatrix} = t_{11}^0; \quad \begin{pmatrix} 5 \\ dd \end{pmatrix} = \frac{t}{4} \begin{pmatrix} 0 \\ 1 \end{pmatrix}^2; \quad (A39)$$

$$\begin{pmatrix} 6 \\ ss \end{pmatrix} = t_{11}^0; \quad \begin{pmatrix} 6 \\ dd \end{pmatrix} = \frac{t}{4} \begin{pmatrix} 0 \\ 1 \end{pmatrix}^2; \quad (A40)$$

$$\begin{pmatrix} 6 \\ pp \end{pmatrix} = \frac{t}{2} \begin{pmatrix} 0 \\ 1 \end{pmatrix}^2; \quad (A41)$$

$$\begin{pmatrix} 7 \\ dd \end{pmatrix} = \frac{J}{8} X_{=1}^3 + 1 \quad 0 \quad 0 \quad + 2; \quad (A42)$$

$$\begin{pmatrix} 7 \\ pd \end{pmatrix} = \frac{J}{4} X_{=1}^3 + 1 \quad 0 \quad 0 \quad + 2; \quad (A43)$$

$$\begin{pmatrix} 7 \\ pp \end{pmatrix} = \frac{J}{4} X_{=1}^3 + 1 \quad 0 \quad 0 \quad + 2; \quad (A44)$$

$$\begin{pmatrix} 11 \\ dd \end{pmatrix} = \frac{J}{8} \left[\begin{pmatrix} 0 \\ 1 \end{pmatrix} \begin{pmatrix} 0 \\ 3 \end{pmatrix} + 2 X_{=2}^3 + 2 \quad 0 \quad 0 \quad + 2 \right]; \quad (A45)$$

$$\begin{pmatrix} 11 \\ pd \end{pmatrix} = \frac{J}{4} X_{=2}^3 \left[\begin{pmatrix} 0 \\ 1 \end{pmatrix} \begin{pmatrix} 0 \\ 3 \end{pmatrix} + 2 X_{=2}^3 + 2 \quad 0 \quad 0 \quad + 2 \right]; \quad (A46)$$

$$\begin{pmatrix} 11 \\ pp \end{pmatrix} = \frac{J}{4} \left[\begin{pmatrix} 0 \\ 1 \end{pmatrix} \begin{pmatrix} 0 \\ 3 \end{pmatrix} + 2 X_{=2}^3 + 2 \quad 0 \quad 0 \quad + 2 \right]; \quad (A47)$$

$$\begin{pmatrix} 13 \\ ss \end{pmatrix} = 2 t_{=2}^0 X_{=2}^3 + 2; \quad \begin{pmatrix} 13 \\ dd \end{pmatrix} = \frac{t}{2} X_{=2}^3 + 2 \quad 0 \quad 0 \quad + 2; \quad (A48)$$

$$\begin{pmatrix} 13 \\ pp \end{pmatrix} = t_{=2}^0 X_{=2}^3 + 2 \quad 0 \quad 0 \quad + 2; \quad (A49)$$

$$\begin{pmatrix} 14 \\ ss \end{pmatrix} = t_{=2}^0; \quad \begin{pmatrix} 14 \\ ds \end{pmatrix} = \frac{t}{2} \begin{pmatrix} 0 \\ 2 \end{pmatrix}^2; \quad (A50)$$

$$\begin{pmatrix} 14 \\ ps \end{pmatrix} = \frac{t}{2} \begin{pmatrix} 0 \\ 2 \end{pmatrix}^2; \quad \begin{pmatrix} 14 \\ dd \end{pmatrix} = \frac{t}{4} \begin{pmatrix} 0 \\ 2 \end{pmatrix}^2; \quad (A51)$$

$$\begin{pmatrix} 14 \\ pd \end{pmatrix} = \frac{t}{2} \begin{pmatrix} 0 \\ 2 \end{pmatrix}^2; \quad \begin{pmatrix} 14 \\ pp \end{pmatrix} = \frac{t}{2} \begin{pmatrix} 0 \\ 2 \end{pmatrix}^2; \quad (A52)$$

$$\begin{pmatrix} 15 \\ ss \end{pmatrix} = t_{=2}^0; \quad \begin{pmatrix} 15 \\ ps \end{pmatrix} = \frac{t}{2} \begin{pmatrix} 0 \\ 2 \end{pmatrix}^2; \quad (A53)$$

$$\begin{pmatrix} 15 \\ dd \end{pmatrix} = \frac{t}{4} \begin{pmatrix} 0 \\ 2 \end{pmatrix}^2; \quad \begin{pmatrix} 15 \\ pd \end{pmatrix} = \frac{t}{2} \begin{pmatrix} 0 \\ 2 \end{pmatrix}^2; \quad (A54)$$

$$\begin{pmatrix} 15 \\ pp \end{pmatrix} = \frac{t}{2} \begin{pmatrix} 0 \\ 2 \end{pmatrix}^2; \quad (A55)$$

$$\begin{pmatrix} 16 \\ ss \end{pmatrix} = t_{=2}^0 X_{=2}^3 + 2 \quad 0 \quad 0 \quad + 2; \quad \begin{pmatrix} 16 \\ dd \end{pmatrix} = \frac{t}{4} X_{=2}^3 + 2 \quad 0 \quad 0 \quad + 2; \quad (A56)$$

$$\begin{pmatrix} 16 \\ pp \end{pmatrix} = \frac{t}{2} X_{=2}^3 + 2 \quad 0 \quad 0 \quad + 2; \quad (A57)$$

$$\begin{pmatrix} 17 \\ dd \end{pmatrix} = \frac{t}{4} \begin{pmatrix} 0 \\ 3 \end{pmatrix}^2; \quad \begin{pmatrix} 17 \\ pd \end{pmatrix} = \frac{t}{2} \begin{pmatrix} 0 \\ 3 \end{pmatrix}^2; \quad (A58)$$

$$\begin{pmatrix} 17 \\ pp \end{pmatrix} = \frac{t}{2} \begin{pmatrix} 0 \\ 3 \end{pmatrix}^2; \quad (A59)$$

and

$$\begin{aligned}
 !_{dd}^{(1)} &= \frac{(\begin{smallmatrix} 0 \\ 3 \end{smallmatrix})^2 + 2^{\begin{smallmatrix} P \\ =4 \end{smallmatrix}} 3^4 (\begin{smallmatrix} 0 \\ 0 \end{smallmatrix})^2}{2}; \\
 !_{pd}^{(1)} &= \frac{(\begin{smallmatrix} 0 \\ 3 \end{smallmatrix})^2 + 2^{\begin{smallmatrix} P \\ =4 \end{smallmatrix}} 3^4 (\begin{smallmatrix} 0 \\ 0 \end{smallmatrix})^2}{2^{\begin{smallmatrix} P \\ =2 \end{smallmatrix}}}; \\
 !_{pp}^{(1)} &= \frac{(\begin{smallmatrix} 0 \\ 3 \end{smallmatrix})^2 + 2^{\begin{smallmatrix} P \\ =4 \end{smallmatrix}} 3^4 (\begin{smallmatrix} 0 \\ 0 \end{smallmatrix})^2}{2}: \quad (A 51)
 \end{aligned}$$

APPENDIX B: OPTICAL CONDUCTIVITY OF DOPED ANTIFERROMAGNETS

The optical spectrum evaluated by us is determined by following contributions to matrix elements ${}^{(n)}h_{R_i}^{(o);0} \hat{j}_k j_{R=0}^{(o);0} i_{S_{o;o}^{(n)}}(R_i)$ where n labels different contributions,

$$\begin{aligned}
 S_{p_x;is}^{(1)}(0) &= 2it \sum_{=0}^X 0_{+1} = \frac{P-}{2}; \\
 S_{s;p_x}^{(1)}(0) &= 2it \sum_{=0}^X 0_{+1} = \frac{P-}{2}; \\
 S_{d;p_x}^{(1)}(0) &= 2it \sum_{=1}^{X=1} 0_{+1} = (2 \frac{P-}{2}); \\
 S_{p_x;id}^{(1)}(0) &= S_{d;p_x}^{(1)}(0) \quad (B 1)
 \end{aligned}$$

$$\begin{aligned}
 S_{p_x;is}^{(2)}(0) &= 2it \sum_{=1}^X 0_{+1} = \frac{P-}{2}; \\
 S_{s;p_x}^{(2)}(0) &= 2it \sum_{=1}^X 0_{+1} = \frac{P-}{2}; \\
 S_{d;p_x}^{(2)}(0) &= 2it \sum_{=2}^{X=1} 0_{+1} = (2 \frac{P-}{2});
 \end{aligned}$$

$$S_{p_x;id}^{(2)}(0) = S_{d;p_x}^{(2)}(0) \quad (B 2)$$

$$S_{s;is}^{(3)}(\hat{x} \hat{y}) = it \sum_0^0 \quad (B 3)$$

$$S_{s;is}^{(4)}(\hat{x} \hat{y}) = S_{s;is}^{(3)}(\hat{x} + \hat{y}) \quad (B 4)$$

$$\begin{aligned}
 S_{s;p_x}^{(5)}(0) &= 4it \sum_{=1}^0 0_{+1} = \frac{P-}{2}; \\
 S_{d;p_x}^{(5)}(0) &= 4it (\begin{smallmatrix} 0 \\ 1 \end{smallmatrix})^2 = (2 \frac{P-}{2}); \quad (B 5)
 \end{aligned}$$

$$\begin{aligned}
 S_{p_x;is}^{(6)}(0) &= S_{s;p_x}^{(5)}(0); \\
 S_{p_x;id}^{(6)}(0) &= S_{d;p_x}^{(5)}(0) \quad (B 6)
 \end{aligned}$$

$$\begin{aligned}
 S_{s;s}^{(7)}(2\hat{x}) &= 2it \sum_0^0; \\
 S_{s;s}^{(7)}(2\hat{x}) &= S_{s;s}^{(7)}(2\hat{x}) \quad (B 7)
 \end{aligned}$$

$$\begin{aligned}
 S_{p_x;is}^{(8)}(0) &= 4it \sum_{=1}^0 0_{+1} = \frac{P-}{2}; \\
 S_{s;p_x}^{(8)}(0) &= S_{p_x;is}^{(8)}(0); \\
 S_{d;p_x}^{(8)}(0) &= 4it \sum_{=1}^0 (\begin{smallmatrix} 0 \\ 1 \end{smallmatrix})^2 = (2 \frac{P-}{2}); \\
 S_{p_x;id}^{(8)}(0) &= S_{d;p_x}^{(8)}(0): \quad (B 8)
 \end{aligned}$$

For example contributions No. 1 and 2 are related to shortening and elongating strings by the current operator, Fig. 11, while contributions No. 3 and 4 to shifts between next NN sites, Fig. 13 (a) and (b). We have considered processes involving strings of length up to two for matrix elements of the t -term in the current operator and up to one for matrix elements of t^0 and t^{00} terms.

-
- [1] J. Hubbard, *Proc. Roy. Soc. London, Ser. A* 277, 237 (1964), and 281, 401 (1964).
- [2] J. Kanamori, *Progr. Theor. Phys.* 30, 275 (1963).
- [3] B. O. Wells, Z.-X. Shen, A. Matsura, D. M. King, M. A. Kastner, M. G. Reven, and R. J. Birgeneau, *Phys. Rev. Lett.* 74, 964 (1995).
- [4] S. A. Trugman, *Phys. Rev. B* 37, 1597 (1988).
- [5] B. Kyung, and R. A. Ferrell, *Phys. Rev. B* 54, 10125 (1996).
- [6] F. Lemar, and A. A. Alligia, *Phys. Rev. B* 55, 14 092 (1997).
- [7] A. L. Chemyshv, A. V. Dotsenko, and O. P. Sushkov, *Phys. Rev. B* 49, 6197 (1994).
- [8] V. I. Belinicher, A. L. Chemyshv, A. V. Dotsenko, and O. P. Sushkov, *Phys. Rev. B* 51, 6076 (1995).
- [9] J. Bala, A. M. Oles, and J. Zaanen, *Phys. Rev. B* 52, 4597 (1995).
- [10] N. M. Plakida, V. S. Oudovenko, P. Horsch, and A. J. Liechtenstein, *Phys. Rev. B* 55, R11997 (1997).
- [11] V. I. Belinicher, A. L. Chemyshv, and V. A. Shubin, *Phys. Rev. B* 56, 3381 (1997).
- [12] O. P. Sushkov, G. A. Sawatzky, R. Eder and H. Eskes, *Phys. Rev. B* 56, 11769 (1997).
- [13] A. Damascelli, Z. Hussain, and Z.-X. Shen, *Rev. Mod. Phys.* 75, 473 (2003).
- [14] Ronning, F., C. Kim, D. L. Feng, D. S. Marshall, A. G. Loeser, L. L. Miller, J. N. Eckstein, L. Bozovic, and Z.-X. Shen, *Science* 282, 2067 (1998).
- [15] R. Eder and Y. Ohta, *Phys. Rev. Lett.* 72, 2816 (1994).
- [16] C. T. Chen, F. Sette, Y. Ma, M. S. Hybertsen, E. B. Stechel, W. M. C. Foulkes, M. Schluter, S. W. Cheong, A. S. Cooper, L. W. Rupp, B. Batlogg, Y. L. Soo, Z. H. Ming, A. Krol, and Y. H. Kao, *Phys. Rev. Lett.* 66, 104 (1991).
- [17] R. Eder, Y. Ohta, and G. A. Sawatzky, *Phys. Rev. B* 55, R3414 (1997).
- [18] J. G. Storey, J. L. Tallon, G. V. M. Williams, and J. W. Loram, *Phys. Rev. B* 76, 060502(R) (2007).
- [19] Kohsaka, Y., T. Sasagawa, F. Ronning, T. Yoshida, C. Kim, T. Hanaguri, M. Azuma, M. Takano, Z.-X. Shen, and H. Takagi, e-print cond-mat/0209339 (2002).
- [20] J. Chang, Y. Sassa, S. Guerrero, M. Månsson, M. Shi, S. Pailhes, A. Bendounan, R. Möttl, T. Claesson, O. Tjernberg, L. Patthey, M. Ido, N. Morimoto, M. Oda, C. Mudry, and J. Mesot, arXiv:0805.0302.
- [21] S. A. Trugman, *Phys. Rev. Lett.* 65, 500 (1990).
- [22] N. P. Ong, Z. Z. Wang, and J. Clayhold, J. M. Tarascon, L. H. Greene, and W. R. M. C. Innon, *Phys. Rev. B* 35, 8807 (1987).
- [23] H. Takagi, T. Ido, S. Ishibashi, M. Uota, and S. Uchida, and Y. Tokura, *Phys. Rev. B* 40, 2254 (1989).
- [24] R. Eder, Y. Ohta, and T. Shimozato, *Phys. Rev. B* 50, 3350 (1994).
- [25] N. Doiron-Leyraud, C. Proust, D. LeBoeuf, J. Levallois, J.-B. Bonnemaison, R. Liang, D. A. Bonn, W. N. Hardy, and L. Taillefer, *Nature* 447, 565 (2007).
- [26] E. A. Yelland, J. Singleton, C. H. Mielke, N. Harrison, F. F. Balakirev, B. Dabrowski, and J. R. Cooper, *Phys. Rev. Lett.* 100, 047003 (2008).
- [27] A. F. Bangura, J. D. Fletcher, A. Carrington, J. Levallois, M. Nardone, B. Vignolle, P. J. Heard, N. Doiron-Leyraud, D. LeBoeuf, L. Taillefer, S. Adachi, C. Proust, and N. E. Hussey, *Phys. Rev. Lett.* 100, 047004 (2008).
- [28] D. LeBoeuf, N. Doiron-Leyraud, J. Levallois, R. Daou, J.-B. Bonnemaison, N. E. Hussey, L. Balicas, B. J. Ramshaw, R. Liang, D. A. Bonn, W. N. Hardy, S. Adachi, C. Proust, and L. Taillefer, *Nature* 450, 533 (2007).
- [29] R. Eder and Y. Ohta, *Phys. Rev. B* 51, 6041 (1995).
- [30] P. W. Leung, *Phys. Rev. B* 73, 014502 (2006).
- [31] E. Dagotto and J. R. Schrieffer, *Phys. Rev. B* 43, 8705 (1991).
- [32] R. Eder and Y. Ohta, *Phys. Rev. B* 50, 10043 (1994).
- [33] R. Eder, Y. Ohta, and S. Maekawa, *Phys. Rev. Lett.* 74, 5124 (1995).
- [34] M. Voja and K. W. Becker, *Europhys. Lett.* 38, 607 (1997).
- [35] R. Eder and Y. Ohta, *Phys. Rev. B* 51, 11683 (1995).
- [36] K. A. Chao, J. Spalek, A. M. Oles, *Phys. Rev. B* 18, 3453 (1978).
- [37] F. C. Zhang and T. M. Rice, *Phys. Rev. B* 37, 3759 (1988).
- [38] A. Nazarenko, K. J. E. Vos, S. Haas, E. Dagotto, and R. J. Gooding, *Phys. Rev. B* 51, 8676 (1995).
- [39] P. W. Leung, B. O. Wells, and R. J. Gooding, *Phys. Rev. B* 56, 6320 (1997).
- [40] R. Eder and K. W. Becker, *Z. Phys. B* 78, 219 (1990).
- [41] R. Eder, K. W. Becker, *Phys. Rev. B* 44, 6982 (1991).
- [42] R. Eder and P. W. Robel, *Phys. Rev. B* 47, 6010 (1993).
- [43] R. Eder, P. W. Robel, and Y. Ohta, *Phys. Rev. B* 54, R11034 (1996).
- [44] P. W. Robel and R. Eder, *Phys. Rev. B* 58, 15160 (1998).
- [45] J. Inoue and S. Maekawa, *J. Phys. Soc. Jpn.* 59, 2110 (1990).
- [46] M. Voja and K. W. Becker, *Phys. Rev. B* 57, 3099 (1998).
- [47] J. Bonca, S. Maekawa, and T. Tohyama, *Phys. Rev. B* 76, 035121 (2007).
- [48] M. Voja and K. W. Becker, *Phys. Rev. B* 54, 15483 (1996).
- [49] G. Martínez and P. Horsch, *Phys. Rev. B* 44, 317 (1991).
- [50] Z. Liu and E. Manousakis, *Phys. Rev. B* 45, 2425 (1992).
- [51] E. Manousakis, *Phys. Rev. B* 75, 035106 (2007).
- [52] G. F. Reiter, *Phys. Rev. B* 49, 1536 (1994).
- [53] J. Eroles, C. D. Batista, and A. A. Alligia, *Phys. Rev. B* 59, 14092 (1999).
- [54] F. Ronning, K. M. Shen, N. P. Anant, A. Damascelli, D. H. Lu, Z.-X. Shen, L. L. Miller, and C. Kim, *Phys. Rev. B* 71, 94518 (2005).
- [55] K. M. Shen, F. Ronning, W. Mevasana, D. H. Lu, N. J. C. Ingle, F. Baumberger, W. S. Lee, L. L. Miller, Y. Kohsaka, M. Azuma, M. Takano, H. Takagi, Z. X. Shen, *Phys. Rev. B* 75, 075115 (2007).
- [56] J. J. M. Pothuizen, R. Eder, N. T. Hien, M. Matoba, A. A. M. Enosky, and G. A. Sawatzky, *Phys. Rev. Lett.* 78, 717 (1997).
- [57] J. Graf, G. H. Gweon, K. McElroy, S. Y. Zhou, C. Jozwiak, E. Rotenberg, A. Bill, T. Sasagawa, H. Eisaki, S. Uchida, H. Takagi, D. H. Lee, and A. Lanzara, *Phys. Rev. Lett.* 98, 067004 (2007).
- [58] B. P. Xie et al., *Phys. Rev. Lett.* 98, 147001 (2007).
- [59] T. Valla, T. E. Kidd, W.-G. Yin, G. D. Gu, P. D. Johnson,

- son, Z.-H. Pan, and A. V. Fedorov, Phys. Rev. Lett. 98, 167003 (2007).
- [60] Z.-H. Pan, P. Richard, A. V. Fedorov, T. Kondo, T. Takeuchi, S. L. Li, Pengcheng Dai, G. D. Gu, W. Ku, Z. Wang, and H. Ding, arXiv:cond-mat/0610442 (2006).
- [61] J. Chang, S. Pailhes, M. Shi, M. M. Anson, T. Claesson, O. Tjernberg, J. Voigt, V. Perez, L. Patthey, N. Momono, M. Oda, M. Ido, A. Schnyder, C. Mudry, and J. Mesot, Phys. Rev. B 75, 224508 (2007).
- [62] D. S. Inosov, J. Fink, A. A. Kordyuk, S. V. Borisenko, V. B. Zabolotnyy, R. Schuster, M. Knupfer, B. Buchner, R. Follath, H. A. Durr, W. Eberhardt, V. Hinkov, B. Keimer, and H. Berger, Phys. Rev. Lett. 99, 237002 (2007).
- [63] D. E. Eastman and J. L. Freeouf, Phys. Rev. Lett. 34, 395 (1975).
- [64] E. Dagotto, F. Ortolani, and D. Scalapino, Phys. Rev. B 46, 3183 (1992).
- [65] H. Eskes and R. Eder, Phys. Rev. B 54, R14226 (1996).
- [66] C. G. rober, R. Eder, and W. Hanke, Phys. Rev. B 62, 4336 (2000).
- [67] S.-J. Oh, J. W. Allen, I. Lindau, and J. C. Mikkelsen, Jr., Phys. Rev. B 26, 4845 (1982).
- [68] M. M. Zemljic, P. P. Rebovsek, and T. Tohyama, Phys. Rev. Lett. 100, 036402 (2008).
- [69] S. Uchida, T. Ido, H. Takagi, T. Arima, Y. Tokura, and S. Tajima, Phys. Rev. B 43, 7942 (1991).
- [70] J. Hwang, E. J. Nicol, T. Timusk, A. Knigavko, and J. P. Carbotte, Phys. Rev. Lett. 98, 207002 (2007).